RSC Advances

The effect of microstructure and elemental content on corrosion and corrosion inhibition of mild steel in 0.5 M H2SO4 environment

Journal:	*RSC Advances*
Manuscript ID	RA-ART-06-2015-011177.R3
Article Type:	Paper
Date Submitted by the Author:	09-Oct-2015
Complete List of Authors:	Chidiebere, Maduabuchi; Federal University of Technology, Owerri, Chemistry Oguzie, Emeka; Federal University of Technology Owerri, Chemistry Li, Ying; Institute of Metal Research, Chinese Academy of Science Liu, Li; Institute of Metal Research, Chinese Academy of Sciences Alshawabkeh, Akram; Northeastern University, 400 Snell Engineering, 360 Huntington Avenue, Boston, Civil and Environmental Engineering Wang, Fuhui; Institute of Metal Research, Chinese Academy of Science
Subject area & keyword:	Materials < Physical

The effect of microstructure and elemental content on corrosion and corrosion inhibition of mild steel in 0.5 M H_2SO_4 environment

Maduabuchi A. Chidiebere [†‡], Emeka E. Oguzie [‡], Li Liu[†], Ying Li*[†], Akram N. Alshawabkeh[ϕ], Fuhui Wang[†],

[†] *Institute of Metal Research, Chinese Academy of Sciences, 62 Wencui Rd, Shenyang, 110016, China.*

[‡] *Electrochemistry and Materials Science Research Unit, Department of Chemistry, Federal University of Technology, Owerri, PMB 1526, Imo State, Nigeria*

[ϕ] *Department of Civil and Environmental Engineering, Northeastern University, 400 Snell Engineering, 360 Huntington Avenue, Boston, MA 02115, United States*

* Corresponding author: Fax: +86-24-2392-5323; Tel: +86-24-2399-2875
E-mail: liying@imr.ac.cn

ABSTRACT

The influence of composition and surface microstructure on the corrosion behavior of low carbon steel specimens from Nigeria (NCS) and China (CCS) in 0.5 M H_2SO_4 environment has been investigated using electrochemical techniques and surface probe techniques. The corrosion inhibition performance of *Chrysophyllum albidum* extract (CA) and synergistic iodide additives (KI) were as well assessed. The obtained results reveal that NCS was more susceptible to corrosion in uninhibited 0.5 M H_2SO_4 solution than CCS, which presented a more positive surface charge. CA inhibited the corrosion of both specimens, yielding maximum inhibition efficiencies of 89.6% and 48.5% for NCS and CCS respectively, which were further increased to 93.9% and 98.9% on introduction of iodide ions. The corrosion and corrosion inhibition behavior of the carbon steel specimens were influenced by the metal composition and microstructure.

Keywords: Acid Solution; Polarization; EIS; Acid Corrosion; Inhibition; Microstructure.

1. INTRODUCTION

Carbon steels are widely utilized in industrial applications. However, their susceptibility to corrosion when exposed to acidic environments is a significant problem both in research as well as in the industry. Accordingly, numerous studies have focused on the corrosion behavior of these materials. Variations in the corrosion behavior of carbon steels could be due to variations in metal surface microstructure, often arising from differences in elemental composition and/or the type of processing/treatment or even grain size modification.[1] In terms of materials corrosion behavior however, microstructure modification yields conflicting outcomes (either improved [2 - 4] or reduced [5, 6] corrosion resistance), depending on the nature of the material and environment.

Sufficient attention has as well been devoted to development of novel and more effective corrosion mitigation measures, including application of corrosion inhibitors, which remains one of the most practical and effective ways for the protection of metallic surfaces in acidic environments. Several organic compounds, as well as biomass extracts have proven to be effective in the corrosion inhibition of carbon steels in an acidic environment.[7 – 24] and usually function via adsorption on the corroding metal surface. [26] The structural, mechanical, and chemical characteristics of the adsorbed layers formed depend on a number of factors, including the electronic structure of the inhibitor, nature of the metal surface and environmental conditions. [27] The corrosion inhibition efficacy of the biomass extracts is attributable to the presence of several organic constituents whose electronic structures bear close resemblance to those of conventional inhibitors. [28]

Investigating the effect of microstructure modifications on the response of metals to corrosion inhibition treatments is an important area of study, which has not received the required attention. A number of studies have investigated corrosion inhibitor performance as a function of metal surface grain size and grain boundary effects. [29 - 33] For instance, thiourea has been reported to act as an effective corrosion inhibitor for both polycrystalline and nanocrystalline iron surfaces in sulfuric acid environment, functioning as a cathodic inhibitor for former and a mixed type inhibitor for the later. [29] Similar studies relating inhibitor performance and metal composition are not very common in the literature.

In order to provide more insight on the influence of alloy composition on the rate and mechanism of carbon steel corrosion in acidic environment, the present study compares the acid corrosion and corrosion inhibition susceptibilities of two carbon steel specimens, commonly used in steel fabrications and structures in Nigeria (Nigerian carbon steel; NCS) and China (Chinese carbon steel; CCS). The response of each system to corrosion inhibitor treatment was assessed using ethanol extracts of *Chrysophyllum albidum* (CA) leaves as inhibitor, as well as CA + KI (potassium iodide) combinations.

2.0. Experimental

2.1. Preparations

The carbon steel specimens used for this study were obtained from Nigeria (Nigeria carbon steel; NCS) and China (China carbon steel; CCS), with percentage composition given in Table 1. The specimens were wet-polished with silicon carbide abrasive paper (from grade #150 – #1000), degreased in acetone and dried in warm air.

The aggressive solution was 0.5 M H_2SO_4 prepared from analytical reagent grade concentrated acid (Sinopharm Chemical Reagent Co., Ltd) using distilled water. The stock solution of *Chrysophyllum albidum* extract (CA) was prepared by boiling weighed amounts of the dried and ground leaves of CA in ethanol under reflux for 3 h. The obtained solution was cooled and filtered. From the resulting filtrate (stock solution), inhibitor test solutions were prepared from the resulting filtrate by serial dilution, using the corrodent as solvent. Corrosion inhibition synergism was assessed by introducing 0.5 mM KI into the inhibited solutions.

2.2. Electrochemical measurements

Electrochemical tests were conducted in a conventional three-electrode corrosion cell, using a PAR-2273 Advanced Electrochemical System, coupled to a PC, running on the Powersuite and Powersine software. A platinum sheet and saturated calomel electrode (SCE) served as counter and reference electrodes respectively. Test metal specimens were fixed in epoxy resin with a surface area of 1 cm^2 exposed to the test solution. Measurements were in aerated and unstirred solutions at the end of 1800s of immersion at 30±1 ^oC. Each test was run in triplicate and the mean values of the measured parameters presented.

Impedance measurements were carried out using signal amplitude perturbation of 5 mV at the corrosion potentials (E_{corr}) and frequency range 100 kHz - 0.1 Hz. The resulting impedance data were analyzed using Zsimpwin 3.0 software. Potentiodynamic polarization measurements were performed at a scan rate of 0.333 mV/s and potential range ±250 mV versus corrosion potential. In order to determine the potential of zero

charge of the carbon steel specimens in 0.5 M H_2SO_4, impedance measured at various potentials in the absence and presence of 800 ppm CA.

2.3. Surface characterization

Surface microstructure examination of the as-received NCS and CCS specimens was observed by optical microscopy (Carl Zeiss Axio Z1m) after etching with 4% Nital solution. A digital camera was fitted to the microscope in order to obtain clear photographs.

X-ray diffraction analysis (XPERT PRD Panalytical) was performed using Cu-Kα radiation. The X-ray diffraction analysis was obtained directly on each specimen surface in order to reveal the nature of the phases.

Surface morphological examination of the metal surfaces before and after immersion in selected test solutions was achieved using XL-30FEG scanning electron microscope with energy dispersive x-ray analysis (EDX). Test metal specimens of dimensions 3 x 3 x 0.25 cm^3 were immersed for 4 h in 0.5 M H_2SO_4, in the absence and presence of 800 ppm CA, retrieved, washed carefully with distilled water, dried in cold air and submitted for SEM investigation.

3.0 Results and Discussions

3.1. Structural analysis.

Fig. 1a and b presents the optical microstructure of the NCS and CCS after etching with 4% Nital solution. The present phases depend on chemical composition, thermal and mechanical history.[34] Steels often have predominantly ferritic microstructures due to low

carbon and alloy contents.[35] Accordingly, we observed a greater percentage of ferrite (white areas) compared to pearlite (dark areas) in both samples, though there is evidence of more pearlite in CCS (Fig.1b). Pearlite formation in carbon steel is usually enhanced by sufficiently slow cooling at the eutectoid point in the Fe-C phase diagram (723 °C, eutectoid temperature).[36] Pearlite is known to be tough and when highly deformed, extremely strong. Hence with much pearlite, the carbon steel is hard and strong but not particularly tough.[37] Inspection of the micrographs show relatively coarse large grain size for NCS compared to the CCS. Also the grain boundaries of the former were more exposed, which should promote penetration of the aggressive solution. The X-ray diffraction (XRD) patterns of NCS and CCS reveal no significant phase differences, which imply that the lattice parameters did not change and no new phases were present. Nevertheless, there is evidence of slight difference in the intensity of the peaks at different diffraction positions (Fig.2).

Furthermore, EDX analysis of the un-immersed specimens were carried out at different positions; results revealed that the elemental composition of the metal specimens as shown in Fig. 3a and 3b were somewhat similar, but for the presence of additional elements such as niobium, vanadium, titanium, and aluminum in CCS. The presence of these grain-refining elements (Nb, Vn, Ti, Al) should be responsible for the relatively finer grains in CCS**.** Interestingly, Nb and Ti have the ability to stabilize carbon and also strengthen steels for high temperature service,[38] therefore their presence in CCS accounts for the higher level of corrosion resistance recorded in our findings. [39]

Fig. 4 shows the SEM micrographs of NCS and CCS before, and after immersion in uninhibited and inhibited acid. The images in Fig. 4a show that the metal surfaces

were severely damaged in the absence of the inhibitor due to active dissolution, with NCS showing greater susceptibility to the corrosive attack (Fig. 3a(i)). The inset in each image gives a detailed view of the surface morphology at higher magnification (5X). Again, the relatively coarse-grained morphology of NCS, with large grain boundaries, is obvious and should be responsible for the observed higher corrosion susceptibility. In the presence of CA extract, the metal surfaces present remarkably smooth morphologies as shown in Fig. 4b. This corresponds to reduced aggressiveness of the corrodent on both surfaces and is attributable to the corrosion inhibiting action of the extract. In addition, there is evidence of inhibitor adsorption at the grain boundaries, particularly for NCS. The smoothening effect is more pronounced for NCS.

3.2. Electrochemical results

3.2. 1. Potentiodynamic polarization measurements

Fig. 5 shows typical potentiodynamic polarization curves of NCS and CCS in 0.5 M H_2SO_4. The corresponding polarization parameters are given in Table 2. As can be seen, both specimens exhibit active dissolution with no distinctive transition to passivation within the potential range studied. The shapes of the polarization curves for NCS and CCS are closely similar, suggesting comparable corrosion mechanisms for both specimens. Nonetheless, NCS displays a more negative corrosion potential and higher anodic and cathodic current densities, corresponding to higher corrosion current density (1340 μA cm^{-2} vs. 792.9 μA cm^{-2} for CCS), all of which imply that NCS was more susceptible to corrosion in 0.5 M H_2SO_4 than CCS. The observed variation in corrosion susceptibility results from difference in metal surface microstructure (grain size, grain boundaries etc) and composition. [30, 32]

To assess the effect of CA extract on the polarization behaviour of NCS and CCS in 0.5 M H_2SO_4, tests were conducted in inhibited solutions containing 200 and 800 ppm CA. The corresponding polarization plots are presented in Fig. 6a and 6b respectively. For NCS, addition of CA shifted E_{corr} in the positive direction and notably lowered the current densities of both the cathodic and anodic process, with more pronounced cathodic effect. For CCS the CA effect is somewhat similar, but more subdued. All of the results indicate that CA functioned as a mixed-type inhibitor, with predominant cathodic effect and was much more effective in controlling the corrosion of NCS in 0.5 M H_2SO_4.

The mean values of the corresponding electrochemical parameters such as corrosion potential (E_{corr}), corrosion current density (I_{corr}), cathodic Tafel slopes (b_c) and anodic Tafel slopes (b_a) estimated by extrapolating the Tafel lines are presented in Table 2, with standard deviation ranging from 0.001 to 0.060. The inhibition efficiency was determined using the equation:

$$IE\% = \left(\frac{i_{corr(bl)} - i_{corr(inh)}}{i_{corr(bl)}} \right) x\ 100 \qquad (1)$$

where $i_{corr\ (bl)}$ and $i_{corr\ (inh)}$ represents the corrosion current density in the absence and presence of the inhibitor, respectively. The IE% values presented in Table 2 show maximum values of 89.6% and 48.5% for NCS and CCS respectively. What this means is that the NCS surface is more susceptible to corrosion and as well more responsive to inhibitor action.

3.2.2. Electrochemical Impedance Spectroscopy.

EIS technique provides detailed information into the kinetics of the interfacial electron transfer processes as well as the surface interactions on the electrochemical system. Fig. 7 shows the Nyquist impedance spectra for NCS and CCS in the uninhibited acid. Table 3 lists the corresponding impedance parameters. The plots show single depressed capacitive semicircles over the frequency range studied. The appearance of the capacitive loop is attributable to charge transfer processes across the metal/solution interface and its diameter is related to the interfacial charge transfer resistance (R_{ct}). The plots for the two specimens are similar, indicating similar corrosion mechanisms. However, the smaller size of the semicircle for NCS suggests lower charge transfer resistance (Table 3), hence higher susceptibility to corrosion.

Addition of CA increased the impedance of both NCS and CCS, hence inhibited the corrosion reaction (Fig. 8a and b), without modifying the mechanism of the corrosion process in either system. The impedance spectra were analyzed by fitting to the equivalent circuit model $R_s (Q_{dl}R_{ct})$, used frequently to model the steel/acid interface. [40, 41, 42] In this circuit, the solution resistance is shorted by a constant phase element (CPE) placed in parallel to the charge transfer resistance. The CPE, with impedance given by Eq. 2 below, stands in for a capacitor, to compensate for deviations from ideal dielectric behavior arising from the inhomogeneous nature of the electrode surface.

$$Z_{CPE} = Q^{-1}(j\omega)^{-n} \qquad (2)$$

Q and n stand for the CPE constant and exponent, respectively, $j^2 = -1$ is an imaginary number, and ω is the angular frequency in rad s^{-1} ($\omega = 2\pi f$ when f is the frequency in Hz), CPE can represent resistance ($Z_{CPE} = R$, $n = 0$), capacitance ($Z_{CPE} =$

C, n =1), Warburg impedance (Z_{CPE} = W, n = 0.5), or inductance (Z_{CPE} = L, n = -1). From the data presented in Table 3, it is clear that R_{ct} for both systems increased with CA concentration, implying that the electrode surfaces get more protection. The values of double-layer capacitance (C_{dl}) were determined using the relation;

$$f\left(Z_{im(max)}\right) = \frac{1}{2\pi C_{dl} R_{ct}} \quad (3)$$

The double-layer capacitance (C_{dl}) for both specimens decreased with CA addition, which, alongside the Helmholtz equation (Eq. 4) provides sufficient experimental evidence of inhibitor adsorption. [43, 44]

$$C_{dl} = \frac{\varepsilon \varepsilon_o A}{\delta} \quad (4)$$

In other words, the lower C_{dl} values result from a decrease in the dielectric constant (ε) and/or an increase in the double layer thickness (δ) due to adsorption of organic constituents of CA (with lower dielectric constant than the displaced water molecules) on the metal/solution interface. ε_o is the vacuum permittivity and A the electrode area, Thus higher R_{ct} values at higher CA concentrations indicate enhanced adsorption of the extract constituents on the steel surface, which hinders the corrosion reaction. [45, 46] A quantitative measure of the protective effect obtained by comparing the values of R_{ct} in the absence and presence of the inhibitor as follows:

$$IE\% = \left(\frac{R_{ct(inh)} - R_{ct}}{R_{ct(inh)}}\right) x\, 100 \quad (5)$$

Where R_{ct} and $R_{ct\ (Inh)}$ denote charge transfer resistance in the absence and presence of inhibitor. The obtained inhibition efficiency values are presented in Table 3.

The slight disparities in the computed inhibition efficiency values from i_{corr} and R_{ct} values is attributable to the inherent differences in the features of either technique. For instance, the impedance measurements are carried out on unperturbed metal surfaces (at E_{corr} and minimal current transfer), whereas polarization measurements are accompanied by considerable deformation of the metal surface (with potential scans positive and negative of E_{corr} and considerable current transfer). Accordingly, the measured responses from both systems are not exactly comparable.

3.3. Effect of Halide additives

It is well known, that the anodic dissolution of steel in aqueous environment is hydroxyl ion-accelerated.[20] Due to high hydrophobicity, large ionic radius and low electronegativity, halide ions adsorbs preferentially the metal surface compared to OH^- [47, 48] and hence modifies the rate of the metal dissolution reaction. Such specific adsorption of halide ions not only modifies metal dissolution, but also modifies the nature and rate of metal-inhibitor interactions, often acting in synergy with some organic inhibitors for improved corrosion protection, in the order; $I^- > Br^- > Cl^-$. [49 - 53]

We studied the influence of iodide ions on the corrosion inhibition performance of CA extract on NCS and CCS. Typical potentiodynamic polarization curves for NCS immersed in CA-inhibited 0.5 M H_2SO_4 in the absence and presence of 0.5 mM KI are presented in Fig. 9a and b. Fig. 10 shows similar plots for CCS. The corresponding

polarization parameters are given in Table 2. It is apparent that the introduction of KI improved the inhibition performance of CA on both samples. The addition of KI shifts E_{corr} towards the anodic direction and further decreases the rate of anodic and cathodic reactions. For instance, introduction of KI reduced the corrosion current densities in inhibited solution containing 200 ppm CA from 601.2 μA cm^{-2} to 240 μA cm^{-2} on NCS and from 637 μA cm^{-2} to 41.7 μA cm^{-2} on CCS. For 800 ppm CA, i_{corr} was lowered from 139.1 μA cm^{-2} to 81.2 μA cm^{-2} on NCS and 407.9 μA cm^{-2} to 8.1 μA cm^{-2} in the presence of KI. Accordingly, the inhibition efficiency (η%) further increased in the presence of KI; from 89.6% to 93.9% for 800 ppm CA on NCS and from 48.5% to 98.9% on CCS. The data in Table 2 show CA-KI synergism to be more pronounced on the CCS surface, compared to NCS. This trend is opposed to that obtained for CA alone, with CA exhibiting superior performance on NCS compared to CCS.

The impedance response of the steel/acid interface in CA-inhibited acid in the absence and presence of KI are presented as Nyquist plots in Fig. 11. The obtained impedance parameters are presented in Table 3. In agreement with the polarization results, the addition of KI increased the size of the Nyquist semicircle for both specimens, yielding higher values of R_{ct} as well as IE% than observed with CA alone. Moreover, C_{dl} values were further reduced, suggesting improved adsorption of the inhibiting species on the metal surfaces. Also, it can be seen that CA+KI was more favourably adsorbed on CCS, whereas CA alone favoured adsorption on NCS.

It is important to note that adsorption of organic inhibitors on a corroding metal surface depends on such factors as; the nature of the aggressive environment, microstructure and surface charge of the metal in the aggressive environment as well as

inhibitor structure and composition of the inhibitor. [54] Of all these, the key variable in the present study is the microstructure and surface charge of the metal. We thus performed experiments to determine the surface charge on NCS and CCS by measuring the potential of zero charge (E_{PZC}) of both carbon steel specimens in 0.5 M H_2SO_4., The charge on a metal surface can be estimated by comparing the potential of zero charge (E_{PZC}) and the open circuit potential (E_{OCP}) of the metal in solution. [55]

$$(\varphi) = (E_{OCP} - E_{PZC}) \quad (5)$$

where φ is the Antropov's rational corrosion potential.

The potential of zero charge (E_{PZC}) of NCS and CCS was evaluated from potential-dependent EIS experiments. Impedance was measured at 100 Hz in 5 mV steps at each applied potential. Fig. 12 illustrates the plots of C_{dl} versus E for both specimens. The minima of the curves represent the E_{PZC} values of the electrodes: - 492 mV and - 550 mV, for NCS (Fig. 12a) and CCS (Fig. 12b). The E_{PZC} values differ by about 58 mV and are both more negative than the corresponding E_{corr} values of – 465.8 mV and – 461.2 mV, respectively, suggesting that electrodes had positive surface charge at the corrosion potential. However, CCS exhibited a more positive charge value (φ = 88.8 mV) compared to NCS (φ = 26.2 mV).

.

In the 0.5 M H_2SO_4 solution, CA will contain both protonated and non-protonated constituents, all of which contribute to the corrosion inhibiting action of the extract. The more positive surface charge on CCS hinders adsorption of protonated extract species, which should be responsible for the comparatively poor performance of CA on this surface, with inhibition efficiency of 19.6% (at 100 ppm) compared to 55% for NCS.

In considering CA-KI synergy, the iodide ions (I^-) are strongly adsorbed on the positively charged metal surface ($M^{\delta+}$) in the acidic media and thereby facilitate adsorption of the protonated constituents of CA ($^{+\delta}_{.}CA$) by acting as intermediate bridges between the positive end of the inhibitor and the positively charged metal surface:

$$\left\| M^{\delta+} - I^- \leftarrow {}^{+\delta}_{.}CA \right\|$$

The CA is then drawn into the double layer by electrostatic interaction with the adsorbed I^- ions, forming ion pairs on the metal surface which increases the degree of surface coverage. [53]

The more pronounced corrosion inhibition synergism realized on the CCS surface is attributable to its more positive surface charge, which obviously favours adsorption of iodide ions, hence increasing the population of corrosion inhibiting ion pairs on the metal surface. This phenomenon is responsible for the remarkable synergistic increase in efficiency from 19.6 to 94.7% (at 100 ppm CA) and from 48.5 to 98.9 % (at 800 ppm CA).

4. CONCLUSIONS

EIS and potentiodynamic polarization studies reveal that both specimens have similar corrosion mechanism in 0.5 M H_2SO_4 solution. The obtained results reveal that NCS was more prone to corrosion in uninhibited 0.5 M H_2SO_4 solution than CCS, which presented a more positive surface charge. CA proved to be an effective inhibitor, and inhibited the corrosion of both specimens, yielding maximum inhibition efficiencies of

89.6% and 48.5% for NCS and CCS respectively, which were further increased to 93.9% and 98.9% on introduction of iodide ions. The more pronounced corrosion inhibition synergism realized on the CCS surface is attributable to its more positive surface charge. Furthermore, the corrosion and corrosion inhibition behavior of the carbon steel specimens were significantly influenced by the metal composition and microstructure.

ACKNOWLEDGEMENTS

M. A. Chidiebere is grateful to the Chinese Academy of Sciences (CAS) and the Academy of Sciences for the Developing World (TWAS) for the award of CAS-TWAS Fellowship. Wenliang Tian and Meijiang Meng are also acknowledged for technical assistance in performing some measurements.

REFERENCES

1. O.O. Joseph, F.I. Alo, An Assessment of the Microstructure and Mechanical Properties of 0.26% Low Carbon Steel under Different Cooling Media: Analysis by one-way ANOVA Industrial Engineering Letters, 2014, 4;

2. C.T. Kwok, F.T. Cheng, H.C. Man, W.H. Ding, *Mater. Lett.,* 2006, **60,** 2419 - 2422.

3. X.Y. Wang, D.Y. Li, *Electrochim. Acta.,* 2002, **47,** 3939 - 3947.

4. K.M.S. Youssef, C.C. Koch, P.S. Fedkiw, *Corros. Sci.,* 2004, **46,** 51- 64.

5. R. Mishra, R. Balasubramaniam, *Corros. Sci.,* 2004, **46,** 3019 - 3029.

6. R. Rofagha, R. Langer, A.M. El-Sherik, U. Erb, G. Palumbo, K.T. Aust, *Scr. Metall. Mater.,* 1991, **25,** 2867 - 2872.

7. C.B. Shen, S.G. Wang, H.Y. Yang, *Appl. Surf. Sci.,* 2006, **253,** 2118 - 2122.

8. M.A. Chidiebere, E.E. Oguzie, L. Liu, Y. Li, F Wang, *Mater. Chem.and Phy.,* 2015, **156**, 95-104.

9. M.A. Quraishi, D. Jamal, *Corros.,* 2000, **56**, 156 - 160.

10. K.F. Khaled, N. Hackerman, *Electrochim. Acta.,* 2003, **48,** 2715 - 2723.

11. S.A. Ali, M.T. Saeed, S.U. Rahman, *Corros. Sci.,* 2003, **45,** 253 - 266.

12. E.E. Oguzie, *Pigm. Resin Technol.,* 2005, **34,** 321- 326.

13. E.E. Oguzie, *Mater. Chem.and Phys.,* 2006, **99,** 441- 446.

14. M.A. Chidiebere, C.E. Ogukwe, K.L. Oguzie, C.N. Eneh, E.E. Oguzie, *Ind. Eng. Chem. Res.,* 2012, **51,** 668 - 677.

15. A. Ostovari, S.M. Hoseinieh, M. Peikari, S.R. Shadizadeh, S.J. Hashemi, *Corros. Sci.,* 2009, **51**, 1935 - 1949.

16. S.A. Umoren, I.B. Obot, N.O. Obi-Egbedi, *J. Mater. Sci.,* 2009, **44,** 274 - 279.

17. P. Bothi Raja, M.G. Sethuraman, *Mater. Lett.,* 2008, **62,** 2977 - 2979.

18. T. Murakawa, T. Kato, S. Nagaura, N. Hackerman, *Corros. Sci.,* 1968, **8,** 483 - 489.

19. Y.C. Wu, P. Zhang, H.W. Pickering, D.L. Allara, *J. Electrochem. Soc.,* 1993, **140**, 2791- 2800.

20. E.E. Oguzie, *Mater. Chem. Phys.,* 2004, **87,** 212 - 217.

21. E.E. Oguzie, Y. Li, F.H. Wang, *J. Colloid Inter. Sci.*, 2007, **310,** 90 - 98.

22. A. Popova, E. Sokolova, S. Raicheva, M. Christov, *Corros. Sci.,* 2003, **45,** 33 - 58.

23. M. Guan Nan, X. Li, F. Li, *Mater. Chem. Phys.,* 2004, **86,** 59 - 68.

24. N. Bouklah, B. Hammouti, A. Aouniti, M. Benkaddour, A. Bouyanzer, *Appl. Surf. Sci.,* 2006, **252,** 6236 - 6242.

25. E.E. Oguzie, Y. Li, F.H. Wang, *Electrochim. Acta.,* 2007, **53**, 909–914.

26. E. E. Oguzie, Z. O. Iheabunike, K. L. Oguzie, C. E. Ogukwe, M. A. Chidiebere, C. K. Enenebeaku, and C. O. Akalezi, *J. Disp. Sci.* Tech., 2013, **34,** 51613, .

27. E.E. Oguzie, C.B. Adindu, C.K. Enenebeaku, C.E. Ogukwe, M.A. Chidiebere, K.L. Oguzie, *J.phys. Chem. C.,* 2012, **116,** 13603 - 13615.

28. S. B. Ulaeto, U. J. Ek pe, M. A. Chidiebere, E. E. Oguzie, *Int. J. of Mat. Chem.,* 2012, **2,** 158-164.

29. S. A. Umoren, Y. Li, F. H. Wang, *Appl Electrochem.,* 2011, **41**, 307–315.

30. E.E. Oguzie, Y. Li, F.H. Wang, *J. Phys. Chem. C.,* 2009, **113,** 8420 - 8429.

31. Y. Li, F. Wang, G. Liu, Corros., 2004, **60,** 891- 896.

32. E.E. Oguzie, Y. Li, F.H. Wang, *Electrochim. Acta.,* 2007, **52,** 6988 – 6996.

33. E.E. Oguzie, Y. Li, F.H. Wang, *J. Sol. Stat. Electrochem.,* 2007, **12,** 721- 728.

34. R.A. Higgins: `Engineering metallurgy', applied physical metallurgy, 6th. Edn, Arnold International Student Edition, London, 1993.

35. L.E. Samuels, `Optical Microscopy of Carbon Steels', American Society for Metals, Metals Park, Ohio, 1980.

36. S.R.Satish Kumar and A.R.Santha Kumar, Design of Steel Structures II, Mesecipres, 2014.

37. A. F Makinde, Ame. J. Mats. Sci., 2011, **1**, 108-112.

38. Muhammad Farooq, 'Strengthening and degradation mechanisms in austenitic stainless steels at elevated temperature, 9th edn, Stockholm, KTH Royal Institute of Technology, 2013, 56.

39. H.E. McGannon, `The Making, Shaping and Treating of Steel', 9th edn, 33. Pittsburgh, Pennsylvania, United States Steel, 1971.

40. I.B. Obot, N.O. Obi-Egbedi, *Corros. Sci.,* 2010, **52,** 198 - 204.

41. Z. Tao, S. Zhang, W. Li, B. Hou, *Ind. Eng. Chem. Res.,* 2011, **50,** 6082 - 6088.

42. M. Kissi, M. Bouklah, B. Hammouti, M. Benkaddour, *Appl. Surf. Sci.,* 2006, **252,** 4190 - 4197.

43. S.M.A. Shibli, V.S. Saji, *Corros. Sci.,* 2005, **47,** 2213 - 2224.

44. A. Saviour Umoren, M.G. Zuhair, I.B. Obot, *Ind. Eng. Chem. Res.,* 2013, **52,** 14855 - 14865.

45. R.A. Prabhu, T.V. Venkatesha, A.V. Shanbhag, B.M. Praveen, G.M. Kulkarni, R.G. Kalkhambkar, *Mater. Chem. Phys.,* 2008, **108,** 283 - 289.

46. G. Moretti, F. Guidi, G. Grion, *Corros. Sci.,* 2003, **46,** 387 - 403.

47. E.E. Ebenso, *Mater. Chem. Phys.,* 2003, **79,** 58 -70.

48. M.A. Chidiebere, E.E. Oguzie, L. Liu, Y. Li, F. Wang, *Ind. Chem. Res.,* 2014, **53,** 7670 – 7679.

49. S.A. Umoren, M.M. Solomon, *J. Ind. Eng. Chem.,* 2015, **21,** 81 –100.

50. U.M. Eduok, S.A. Umoren, A.P. Udoh, *Arab J of Chem.,* 2012, **5,** 325–337**.**

51. A. I. Onen and B. T. Nwufo, *J. Chem. Soc. Nig.,* 2010, **35,** 145-156.

52. O. A. Hazazi, A. Fawzy, M. Awad, *Int. J. Electrochem. Sci.,* 2014, **9,** 4086 – 4103.

53. R.T. Loto, C.A. Loto, A.P.I. Popoola, *J. Mater. Environ. Sci.,* 2012, **3,** 885 – 894.

54. L.I. Antropov, E.M. Makushin, V.F. Panasenko, Metal Corrosion Inhibitors,*Technika, Kiev*, 1981, 182.

55. I.B. Obot, *Port. Electrochim. Acta.,* 2009, **27**, 539-553.

Figures and Captions

Fig. 1 Optical micrographs of: (a) NCS and (b) CCS

Fig. 2 XRD patterns for: (a) NCS and (b) CCS.

Fig. 3 SEM micrographs of: a(i) freshly polished NCS, a(ii) accompanying EDX spectra, b(i) freshly polished CCS d(ii) accompanying EDX spectra.

Fig. 4 SEM micrographs of: a(i) NCS in uninhibited acid a(ii) CCS in uninhibited acid, b(i) NCS in CA-inhibited acid, b(ii) CCS in CA-inhibited acid. The inset represents the surface morphologies at higher magnification (5X).

Fig. 5 Typical polarization curves of NCS and CCS in uninhibited 0.5 M H_2SO_4

Fig. 6 Potentiodynamic polarization curves of: (a) NCS and (b) CCS in 0.5 M H_2SO_4 in the absence and presence of different concentrations of CA

Fig. 7 Electrochemical impedance (Nyquist) plots of NCS and CCS in uninhibited 0.5 M H_2SO_4

Fig. 8 EIS Nyquist plots of: (a) NCS and (b) CCS in 0.5 M H_2SO_4 solution in the absence and presence of different concentrations of CA.

Fig. 9 Potentiodynamic polarization plots of NCS in 0.5 M H_2SO_4 showing effect of 0.5 mM KI additives on the performance of: (a) 200 ppm CA and (b) 800 ppm CA.

Fig. 10 Potentiodynamic polarization plots of CCS in 0.5 M H_2SO_4 showing effect of 0.5 mM KI additives on the performance of: (a) 200 ppm CA and (b) 800 ppm CA.

Fig. 11 Nyquist plots of (a) NCS and (b) CCS in 0.5 M H_2SO_4 solution in the absence and presence of different concentrations of CA and with 0.5 mM KI.

Fig. 12 Capacitance vs. voltage plots of: (a) NCS and (b) CCS in 0.5 M H_2SO_4 solution.

Tables and Captions

Table 1 Chemical composition of NCS and CCS

Table 2 Polarization parameters for NCS and CCS in 0.5 M H_2SO_4 in the absence and presence of CA and CA + 0.5 mM KI

Table 3 Electrochemical impedance parameters for NCS and CCS in 0.5 M H_2SO_4 in the absence and presence of CA and CA + 0.5 mM KI

Table 1 Chemical composition of NCS and CCS

	C	Si	Al	P	Ti	Nb	V	S	Fe
NCS	0.15	0.21	-	0.0035	-	-	-	-	Bal.
CCS	0.16	0.28	0.025	0.045	0.04	0.0012	0.0036	0.050	Bal.

Table 2 Polarization parameters for CCS and NCS in 0.5 M H_2SO_4 in the absence and presence of CA and CA + 0.5 mM KI

System	E_{corr} (mV vs SCE)	I_{corr} (μA cm^{-2})	b_c (mV dec^{-1})	b_a (mV dec^{-1})	IE (%)
NCS					
Blank	- 465.8	1340	204.2	135.7	
200 ppm CA	- 473.9	601.2	202.7	110.5	55.1
800 ppm CA	- 462.2	139.1	202.2	87.1	89.6
200 ppm CA + 0.5 mM KI	- 462.7	240	164.1	60.2	82.1
800 ppm CA + 0.5 mM KI	- 428.7	81.2	177.4	20.4	93.9
CCS					
Blank	- 461.2	792.9	181.2	119.5	
200 ppm CA	-463	637	196.4	67	19.6
800 ppm CA	-467.3	407.9	160.7	72.4	48.5
200 ppm CA + 0.5 mM KI	-419.2	41.7	157	67.7	94.7
800 ppm CA + 0.5 mM KI	-391.7	8.1	154.8	59.4	98.9

Table 3 Electrochemical impedance parameters for NCS and CCS in 0.5 M H_2SO_4 in the absence and presence of CA and CA + 0.5 mM KI

System	R_{ct} (Ω cm^2)	n	C_{dl} (μF cm^{-2})	IE (%)
NCS				
Blank	8.02	0.91	100.5	
200 ppm CA	30.1	0.90	61.1	73.3
800 ppm CA	269.9	0.80	55.9	97
200 ppm CA + 0.5 mM KI	47.09	0.90	35.6	83
800 ppm CA + 0.5 mM KI	581.8	0.87	18	98.6
CCS				
Blank	41.1	0.88	112.8	
200 ppm CA	49.9	0.90	66	17.6
800 ppm CA	63.3	0.90	43.7	35.8
200 ppm CA + 0.5 mM KI	1332	0.90	1.5	97
800 ppm CA + 0.5 mM KI	3124	0.99	0.6	98.6

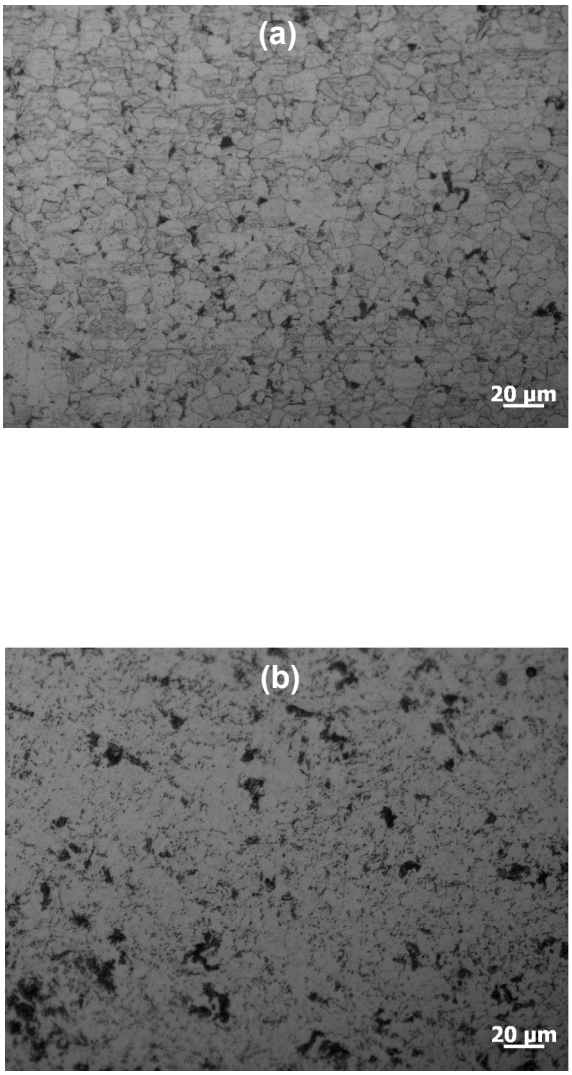

Fig. 1 Optical micrographs of: (a) NCS and (b) CCS

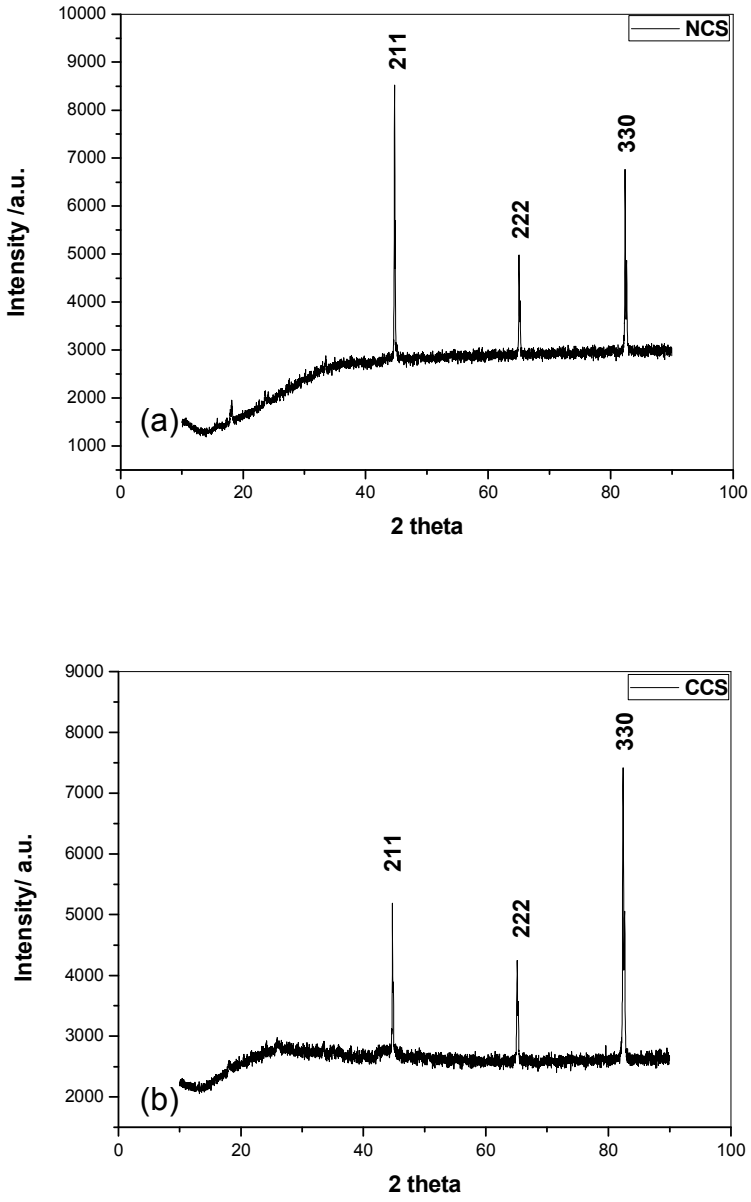

Fig. 2 XRD patterns for: (a) NCS and (b) CCS

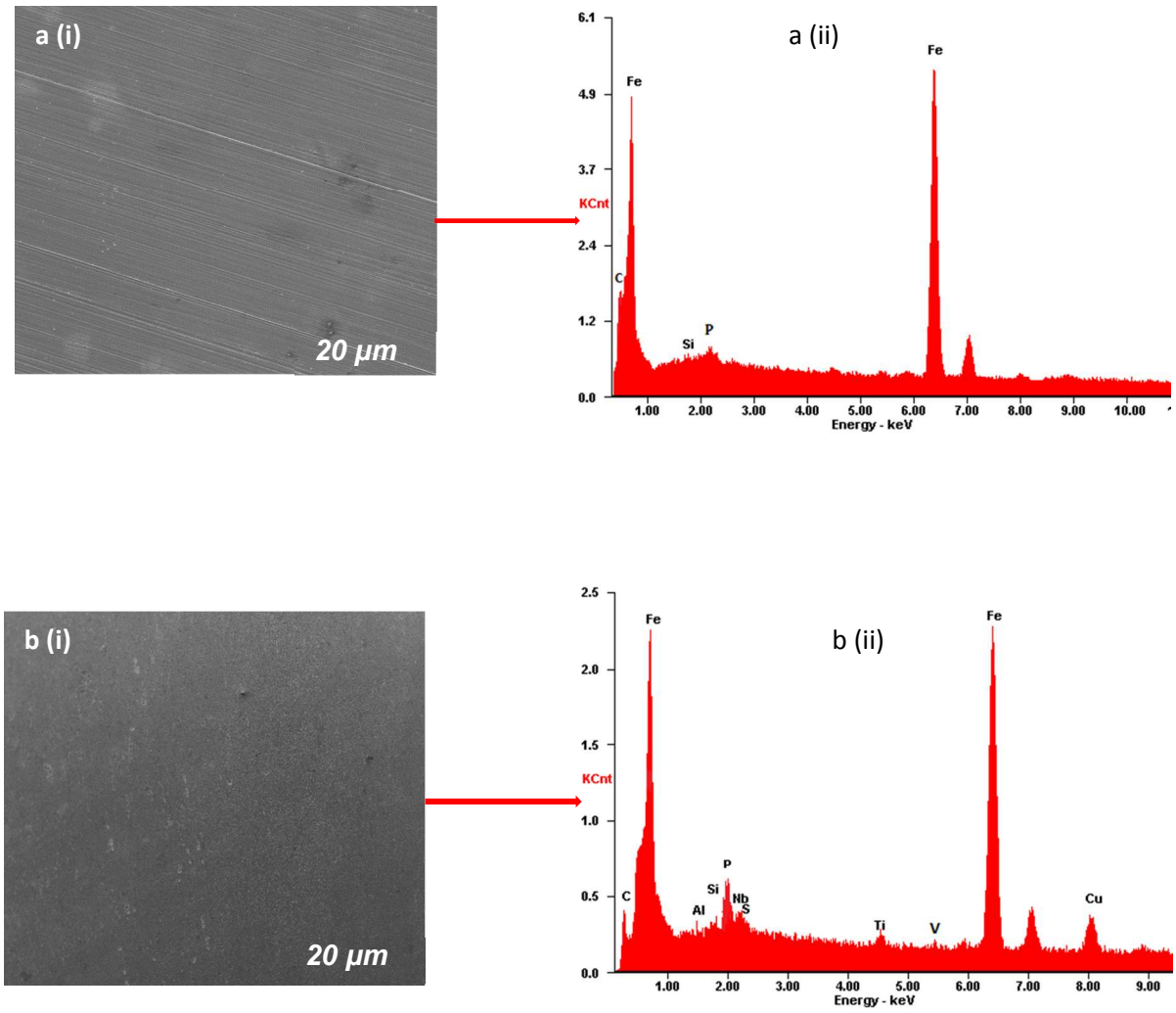

Fig. 3 SEM micrographs of: a(i) freshly polished NCS, a(ii) accompanying EDX spectra, b(i) freshly polished CCS d(ii) accompanying EDX spectra.

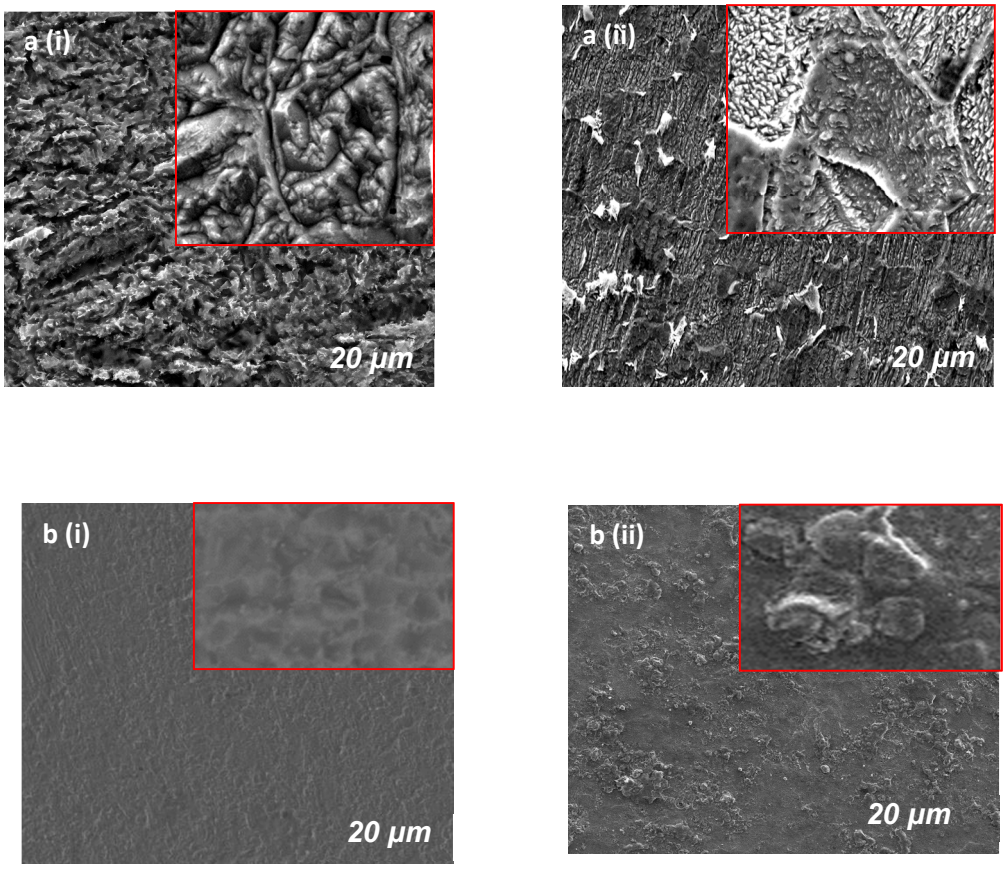

Fig. 4 SEM micrographs of: a(i) NCS in uninhibited acid a(ii) CCS in uninhibited acid, b(i) NCS in CA-inhibited acid, b(ii) CCS in CA-inhibited acid. The inset represents the surface morphologies at higher magnification (5X).

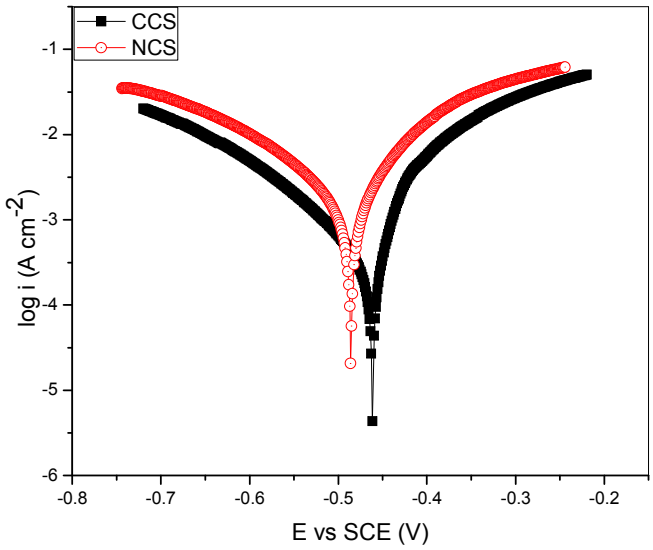

Fig. 5 Typical polarization curves of NCS and CCS in uninhibited 0.5 M H_2SO_4

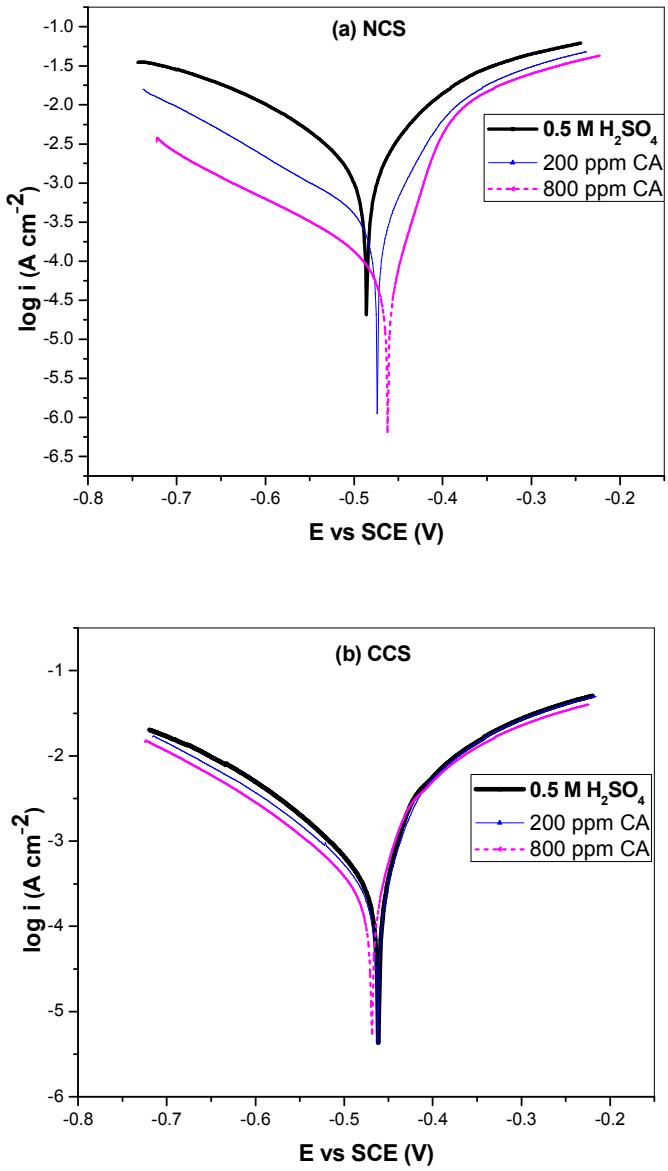

Fig. 6 Potentiodynamic polarization curves of: (a) NCS and (b) CCS in 0.5 M H_2SO_4 in the absence and presence of different concentrations of CA

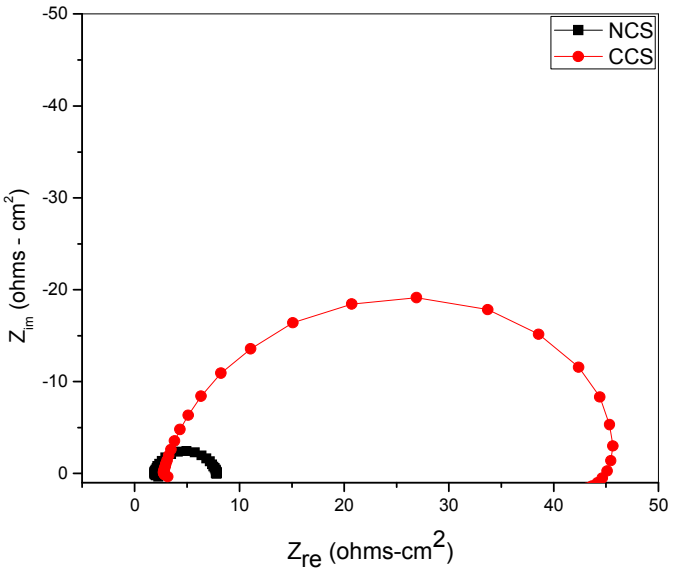

Fig. 7 Electrochemical impedance (Nyquist) plots of NCS and CCS in uninhibited 0.5 M H_2SO_4

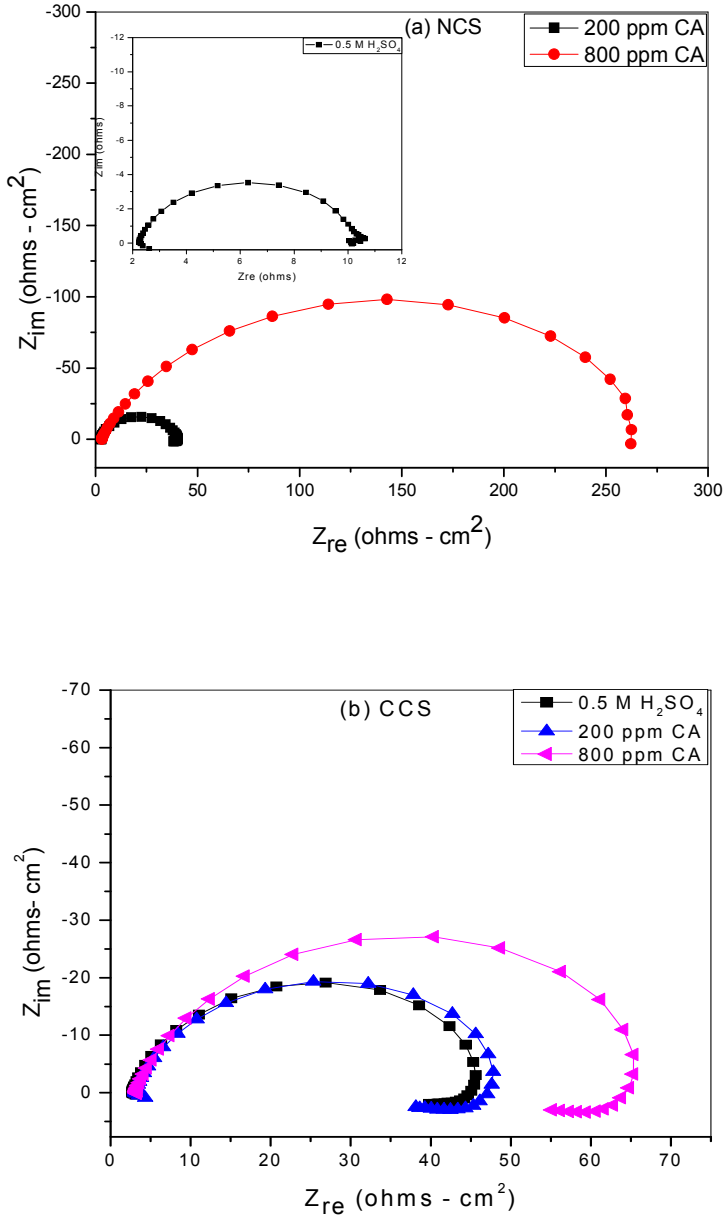

Fig. 8 EIS Nyquist plots of: (a) NCS and (b) CCS in 0.5 M H_2SO_4 solution in the absence and presence of different concentrations of CA.

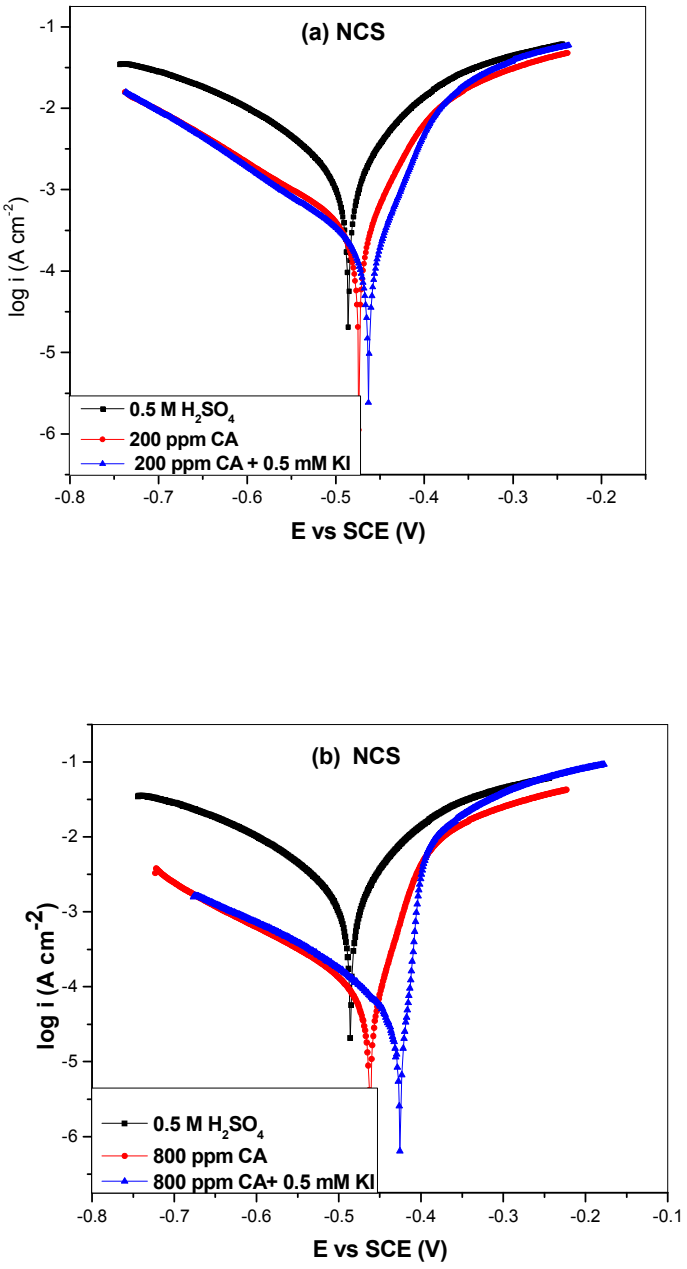

Fig. 9 Potentiodynamic polarization plots of NCS in 0.5 M H_2SO_4 showing effect of 0.5 mM KI additives on the performance of: (a) 200 ppm CA and (b) 800 ppm CA.

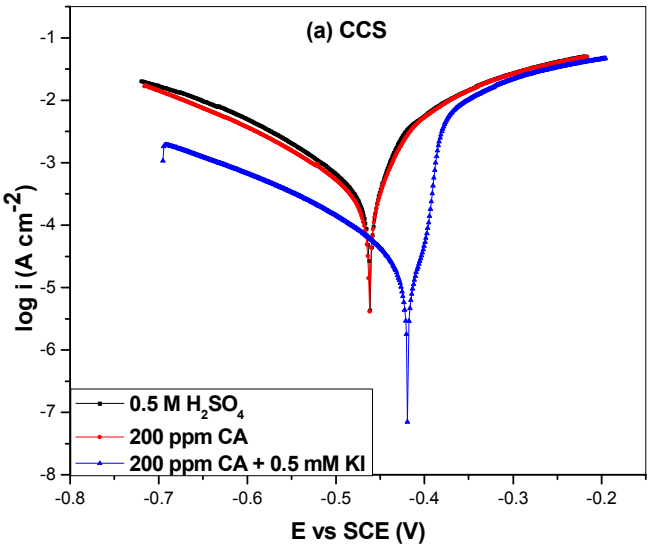

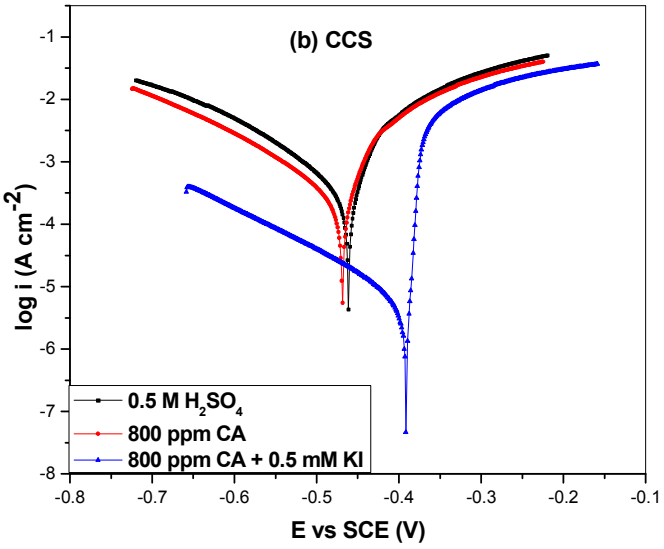

Fig. 10 Potentiodynamic polarization plots of CCS in 0.5 M H_2SO_4 showing effect of 0.5 mM KI additives on the performance of: (a) 200 ppm CA and (b) 800 ppm CA.

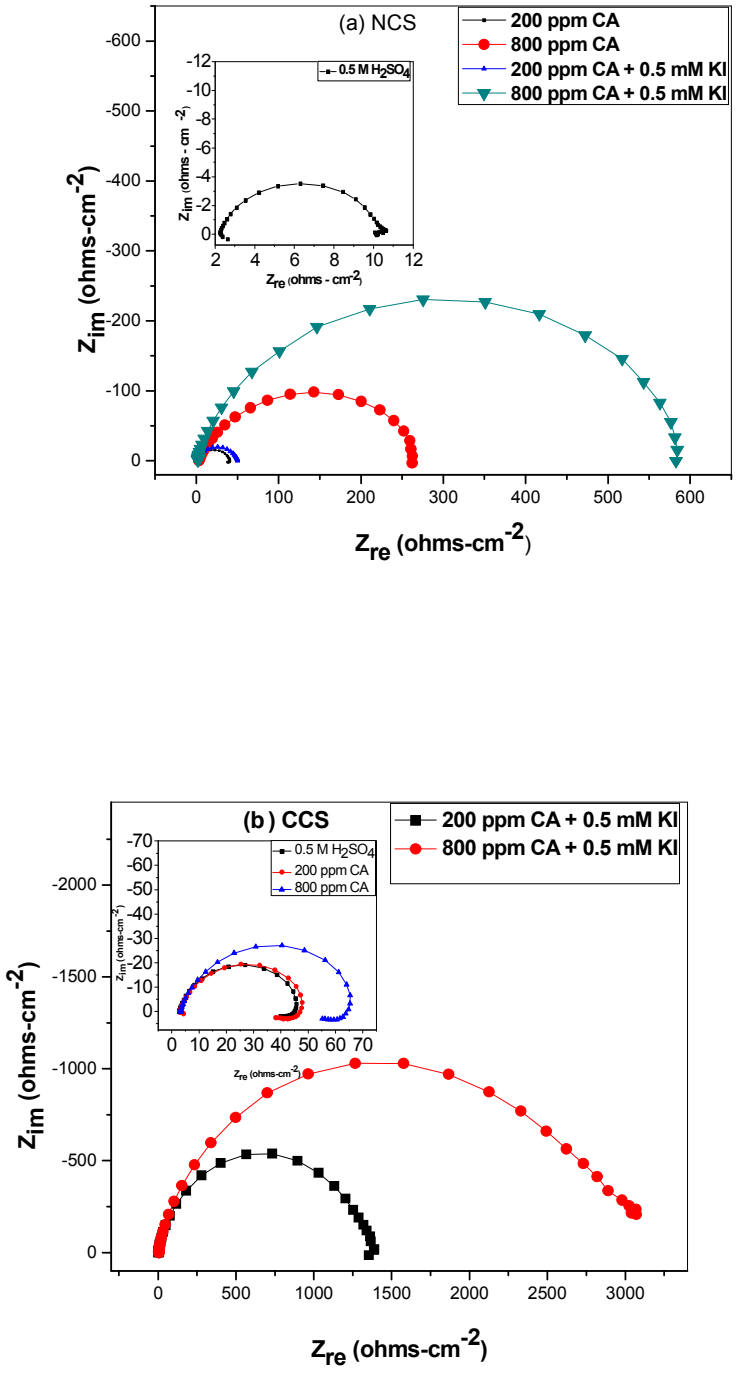

Fig. 11 Nyquist plots of: (a) NCS and (b) CCS in 0.5 M H_2SO_4 solution in the absence and presence of different concentrations of CA and with 0.5 mM KI.

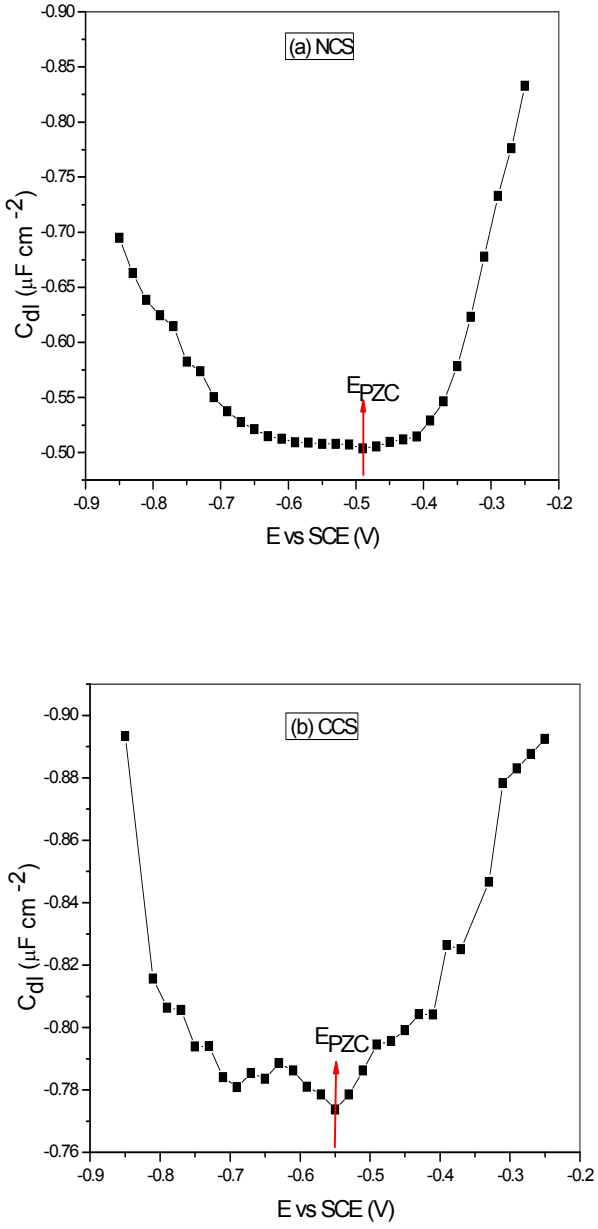

Fig. 12 Capacitance vs. voltage plots of: (a) NCS and (b) CCS in 0.5 M H_2SO_4 solution.